Theoretical and Applied Climatology (2020) 141:1645–1659
https://doi.org/10.1007/s00704-020-03300-6

ORIGINAL PAPER

Impact of air-sea interaction during two contrasting monsoon seasons

Sahil Sharma[1] · Amita Kumari[1] · M. P. Navajyoth[1] · Pankaj Kumar[1] · Md. Saquib Saharwardi[1]

Received: 29 August 2019 / Accepted: 10 June 2020 / Published online: 22 June 2020

Abstract

The air-sea interaction processes and their relation to Indian summer monsoon rainfall via dynamic and thermodynamic components are vital. The present study examined the two contrasting monsoon years 2016 (normal) and 2017 (below normal) and highlighted the significance of air-sea interaction in the understanding the rainfall over central India. We investigate the difference in the sea surface height anomaly and propagation of oceanic Kelvin and Rossby wave over the tropical Indian Ocean and other atmospheric parameters during the contrasting monsoon years. The study gives information on how equatorial and coastal Kelvin/Rossby waves cause upwelling/downwelling and modulate convection and influence rainfall during 2016 and 2017. The high (low) sea surface height anomaly, sea surface temperature, and upper ocean heat content during 2016 (2017) lead to enhanced (subdued) convection in the Bay of Bengal and thereby contributing more rainfall to central India. During 2016 (2017), high (low) tropospheric temperature draws more (less) moisture through mid-tropospheric heat flux, and net convergence (divergence) is dominated over the central India that results in enhanced (diminish) convection. Also, the velocity potential determines the strengthening (weakening) of Walker circulation through associated atmospheric circulation and upper-level divergence (convergence) that become favorable for rainfall in the year 2016 (2017). This study will help in understanding the variations in the air-sea interaction processes over the tropical Indian Ocean and the Indian subcontinent, the results of which may improve the predictability of the rainfall.

1 Introduction

The year-to-year variations of the Indian summer monsoon rainfall (ISMR) over the spatiotemporal scales exert a profound influence on the agricultural production, economy, and human lives in one of the utmost densely inhabited regions of the world (Gadgil et al. 2004). Accurate prediction of the monsoonal rainfall is essential for policy and decision making, yet, the mechanisms underlying the monsoon processes are not entirely comprehended and pose a great challenge for researchers and significant area of research.

Notably, the tropical monsoon framework comprises of air-sea interaction processes and the feedbacks between the two play a vital role in the evolution and modulation of ISMR. Studies that relate ISMR with dynamics of Indian Ocean (IO) by linking the subsurface oceanic to atmospheric processes are gaining much importance (Raju et al. 2002; Rao et al. 2010b; Bhatla et al. 2011; Sreejith et al. 2015; Venugopal et al. 2018). The tropical IO acts as an important part of the tropical monsoon system, and various regions exhibit crucial roles in modulating the ISMR via dynamic and thermodynamic components. The ISMR and its relation with the sea surface temperature (SST) variability over the IO, from a cautious perspective, using satellite-derived SST datasets for two different monsoon years (1979 and 1983) have been examined by Kumar et al. (1986)). They observed a significant correlation between zonal anomaly of SST off the coast of Somalia with the western and central monsoonal rainfall. In another study, Ramesh Kumar et al. (2005)) looked at the air-sea interaction over the tropical IO during contrasting monsoon years 2003 (normal) and 2002 (deficit). They found lower (higher) evaporation rates over the Arabian Sea (AS) during active (weak) monsoon conditions. The formation of a low-pressure system in the Bay of Bengal (BoB) during the active phase is nearly 3.5 times higher than in the break phase. The tracks of these synoptic activities are also firmly spatially bunched along the monsoon trough during the active period of monsoon (Goswami et al. 2003). Most of the

✉ Pankaj Kumar
kumarp@iiserb.ac.in

[1] Indian Institute of Science Education and Research Bhopal, Bhopal, India

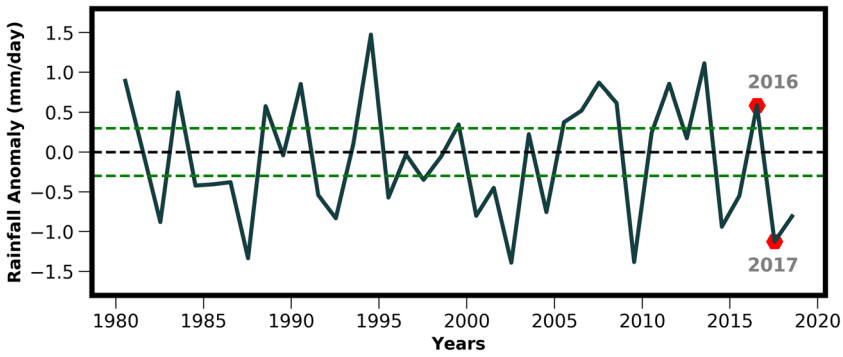

Fig. 1 JJAS rainfall anomaly averaged over the box (16.5 N to 26.5 N, 74.5° E to 86.5° E) from 1979 to 2018. The two green lines represent the criteria for determining strong and weak monsoon years. The red dots represent the two years (2016 and 2017) used in the analysis as two contrasting monsoon years

past studies emphasize SST and air-sea fluxes, and their roles in convection (Gadgil et al. 1984; Krishnamurti et al. 1988; Sengupta and Ravichandran 2001; Sengupta et al. 2001; Vecchi and Harrison 2002; Shankar et al. 2007; Parampil et al. 2010). In recent decades, several researchers examined the influence of air-sea interaction processes such as the Indian Ocean Dipole (IOD) (Saji et al. 1999; Webster et al. 1999; Murtugudde et al. 2000; Ashok et al. 2001; Feng et al. 2001; Rao et al. 2002, 2010a, b; Annamalai et al. 2003) and El-Nino (Walker and Bliss 1932; Sikka 1980; Pant and Parthasarathy 1981; Keshavamurty 1982; Krishnamurthy and Goswami 2000; Ashok et al. 2001; Shukla and Paolino 2002) on the ISMR. ENSO influences the ISMR through equatorial Walker circulation and thus the regional Hadley circulation (Goswami 1998; Webster et al. 1998). The atmospheric component of IOD, EQUINOO (Equatorial Indian Ocean Oscillation), plays an essential role in controlling the ISMR. The upper Ocean Heat Content (OHC) is one of the most important factors for the formation and intensification of the cyclone (Emanuel 1999). The spatiotemporal variations of upper OHC in the BoB concerning the formation and development of cyclones have been the subject of several studies (Sadhuram et al. 2004; Yu and McPhaden 2011; Wang et al. 2012). The low-pressure systems which originate over BoB move westward over the Indian landmass that contributes substantially to the ISMR (Goswami et al. 2003).

The planetary oceanic Kelvin wave (KW) and Rossby wave (RW) plays an important role in the spatial distribution of upper OHC. Both KW and RW help in transportation energy and mass and also influence the currents and surface circulation all over the IO. During monsoon season, the equatorial zonal winds in the IO drive equatorial KW which propagates eastward and radiates westward moving RW on striking the east coast (Potemra et al. 1991; McCreary et al. 1993). On interception by the east coast, the KW bifurcates as southward and northward coastal KW. The latter follows the coastal waveguide of the BoB and travels over a great distance along the coast. The equatorial and coastal KW radiate westward propagating RW (Potemra et al. 1991; McCreary et al. 1993; Masumoto and Meyers 1998; Peter and Mizuno 2000; Rao and Sivakumar 2000; Subrahmanyam et al. 2001; Brandt et al. 2002; Kantha et al. 2008; Chowdary et al. 2009; Schiller et al. 2010; Trenary and Han 2012). The propagation of KW and RW in the ocean can be observed using sea surface height anomaly (SSHA) and are responsible for sea-level fluctuation in all time scales (Chelton and Schlax 1996; Polito 1997). SSHA is a significant parameter to investigate and understand the air-sea interaction like a monsoon, IOD, and ENSO (Meyers 1996; Feng et al. 2001; Feng and Meyers 2003). SSH indicates the vertically integrated density variation in the whole water column and gives information about the thermocline and pycnocline. Changes in the SSH describe the subsurface ocean and ocean-atmosphere interaction parameters such as upper OHC and SST, providing thermodynamic feedback to the atmosphere. Yang et al. (1998)) showed that the seasonal changes in the sea level over the tropical and subtropical IO are primarily due to RW and KW forced by the IO monsoon. Rao et al. (2010a, b) determined that the enhanced convection in the southwest IO and suppression of rainfall over central India during the 2008 drought is primarily due to the advection of

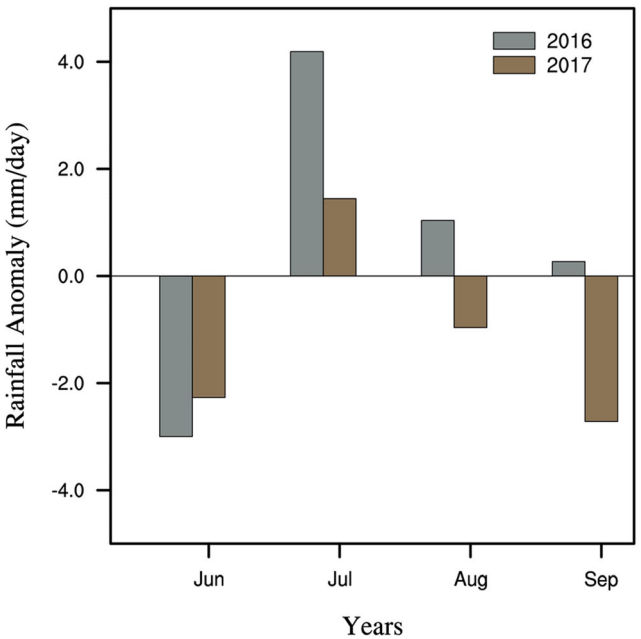

Fig. 2 Monthly JJAS rainfall anomaly averaged over the box (16.5° N–26.5° N and 74.5° E–86.5° E) for the years 2016 and 2017

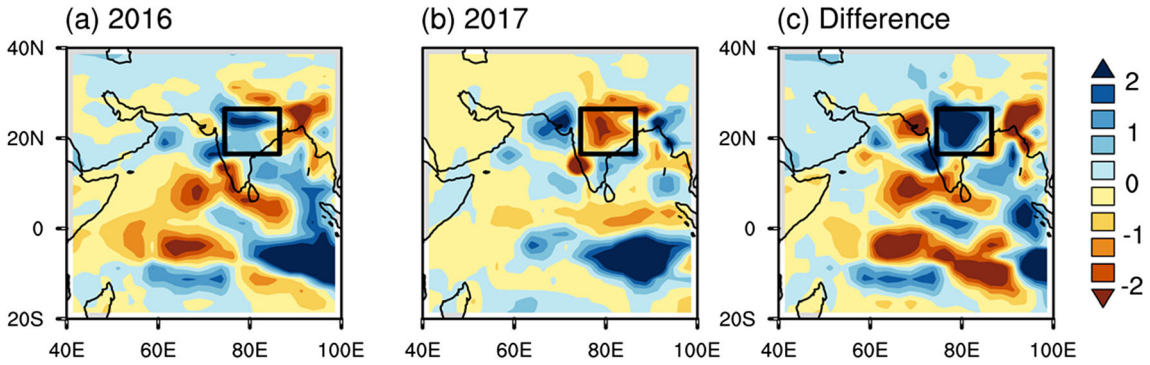

Fig. 3 JJAS rainfall anomalies (mm/day) during **a** 2016, **b** 2017, and **c** difference

oceanic heat by RW. The formation of seasonal eddies in the BoB and AS are substantially linked with the RW generated due to the coastal KW and equatorial RW. In view of the impact of the spatial and temporal variations of SSHA, KW, and RW on ISMR, it is convincing to study their behavior and propagation during contrasting monsoon seasons.

This study considers two contrasting monsoon seasons (2016 and 2017). The 2017 monsoon season rainfall had a deficit of 5% from the long period average (LPA), which was primarily due to a below-normal rainfall activity during the second half of monsoon season (India Meteorological Department 2017). The monthly rainfall was (88%) 87% of LPA in (September) August (India Meteorological Department 2017). Joseph et al. (2018)) determined the dynamics of extended break spells in the latter half of 2017 monsoon. They ascertained an enhanced typhoon activity in the northwestern Pacific and the intrusion of the mid-latitude westerly through to the Indian region detriment the rainfall over the Indian landmass. However, during the 2016 monsoon season, the country received 97% of LPA and experienced more than normal rainfall. The monthly rainfall was 107, 91, and 97% of LPA in July, August, and September respectively (India Meteorological Department 2016). The main objective of the present study is to analyze different air-sea interaction processes during two contrasting monsoon seasons and outline their influence on the rainfall over monsoon core region.

2 Data and methodology

The AVISO merged altimeter SSHA data with weekly records on a 0.25° grid is used to study the sea level variability and the signatures of KW and RW propagation. The altimeter data, unlike the tidal gauge data, provides the spatial distribution of sea level both globally and regionally. Therefore, the altimeter dataset can be extensively used to understand the recent regional sea-level changes in detail. The "all-sat-merged" product acquires data from various satellites and has better spatial resolution and smaller mapping errors than datasets based on a single satellite. Altimeters observe the height of the satellite above the sea surface generally with a precision of ± 2 cm and an accuracy of ± 4 cm. The linear trend is removed while computing SSHA, to avoid any warming trend patterns in the IO as reported by many authors (Alory and Meyers 2009; Han et al. 2010).

Global Precipitation Climatology Project (GPCP) monthly rainfall data is used for spatial and temporal analysis during the two contrasting monsoon years. The data has a horizontal resolution of 2.5°. The criterion used to select the different monsoon years is taken from Gera et al. (2016)). They used a rectangular domain (74.5° E to 86.5° E and 16.5° N to 26.5° N) over the Indian landmass and calculated the JJAS rainfall anomaly over the given box. The years for which the JJAS rainfall anomaly over the box

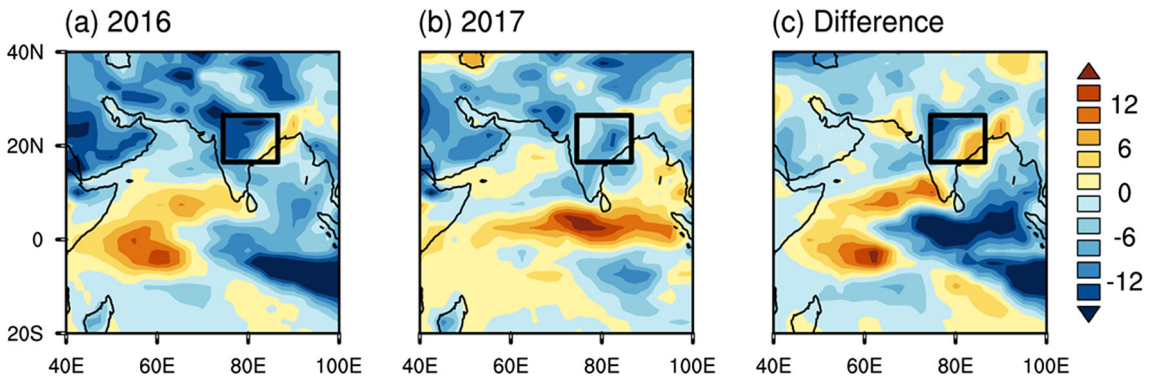

Fig. 4 JJAS OLR anomalies (w/m^2) during **a** 2016, **b** 2017, and **c** difference

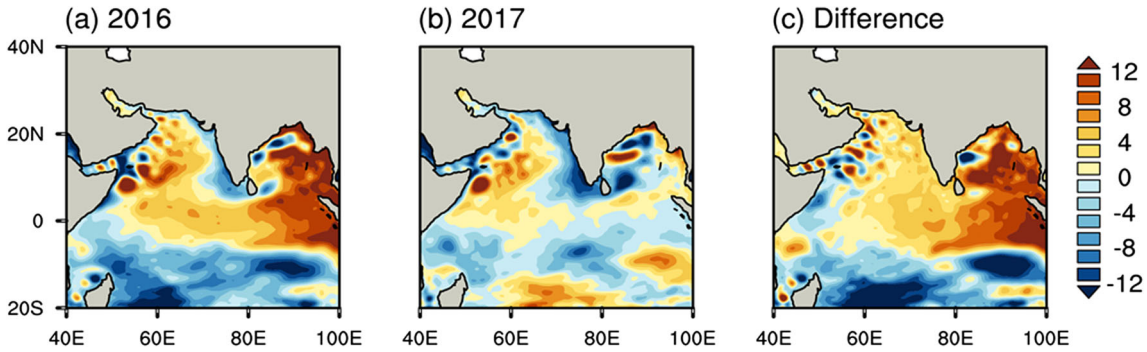

Fig. 5 JJAS SSHA (cm) during **a** 2016, **b** 2017, and **c** difference

is greater (less) than 0.3 mm/day (− 0.3 mm/day) are marked strong (weak) monsoon years. For our analysis of two contrasting monsoon years, i.e., 2016 and 2017, the JJAS rainfall anomalies over the highlighted domain are + 0.55 mm/day and − 1.10 mm/day respectively. The JJAS rainfall variation since 1980 and monthly rainfall anomaly for the years 2016 and 2017 using GPCP dataset are shown in Figs. 1 and 2, respectively. The meteorological parameters utilized from NCEP/NCAR reanalysis to understand the behavior of the atmosphere during the contrasting monsoon years used in the study include outgoing longwave radiation (OLR), zonal and meridional components of wind, velocity potential at 200 hPa, and air temperature at different pressure levels. The moisture transport is computed using the ERA-Interim dataset (zonal wind, meridional wind, and specific humidity). The tropospheric temperature (TT) between 600 and 200 hPa is calculated using the air temperature dataset at various pressure levels. Vertical velocity at various pressure levels and vertically integrated mass convergence/divergence (1000–300 hPa) obtained from ERA-Interim are used in the analysis as well. OHC anomaly at a depth of 0–700 m was obtained from with a spatial resolution of 1° × 1° for the given period from National Oceanography Data Centre (NODC). Anomalies of all the oceanic and atmospheric parameters are calculated with respect to the base period 1993–2012.

3 Results and discussion

3.1 Impact of oceanic parameters during the two contrasting monsoon seasons

In this section, we examine the impact of oceanic parameters on the monsoonal rainfall over the tropical IO and Indian subcontinent during the two contrasting seasons, and probable mechanisms behind.

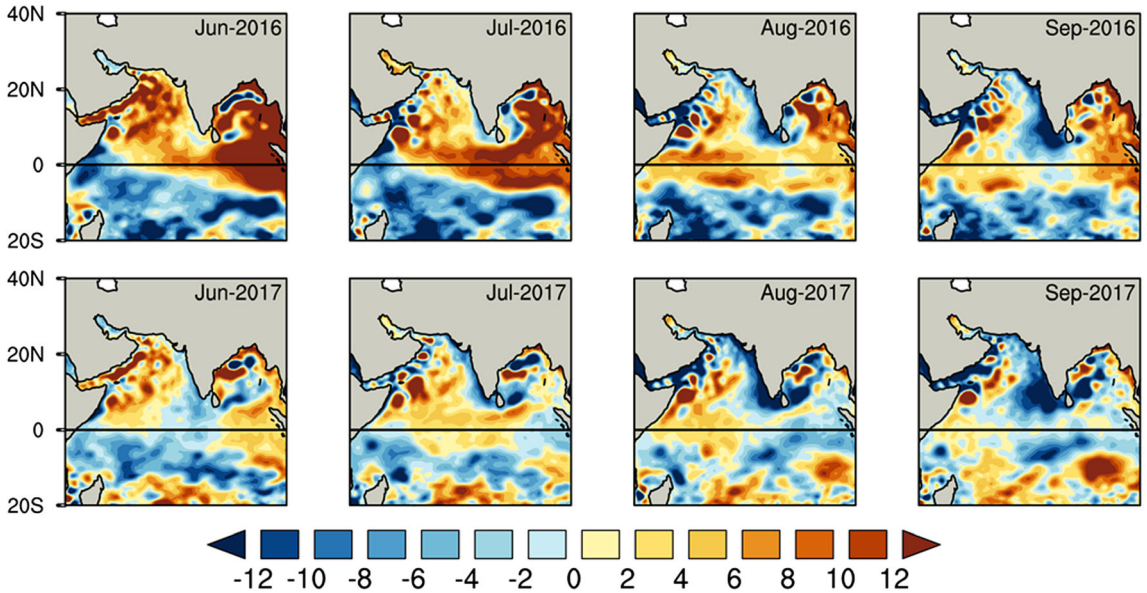

Fig. 6 The upper panel shows the monthly averaged SSHA (cm) from June to September during 2016 and the lower panel depicts the monthly averaged SSHA (cm) from June to September during 2017

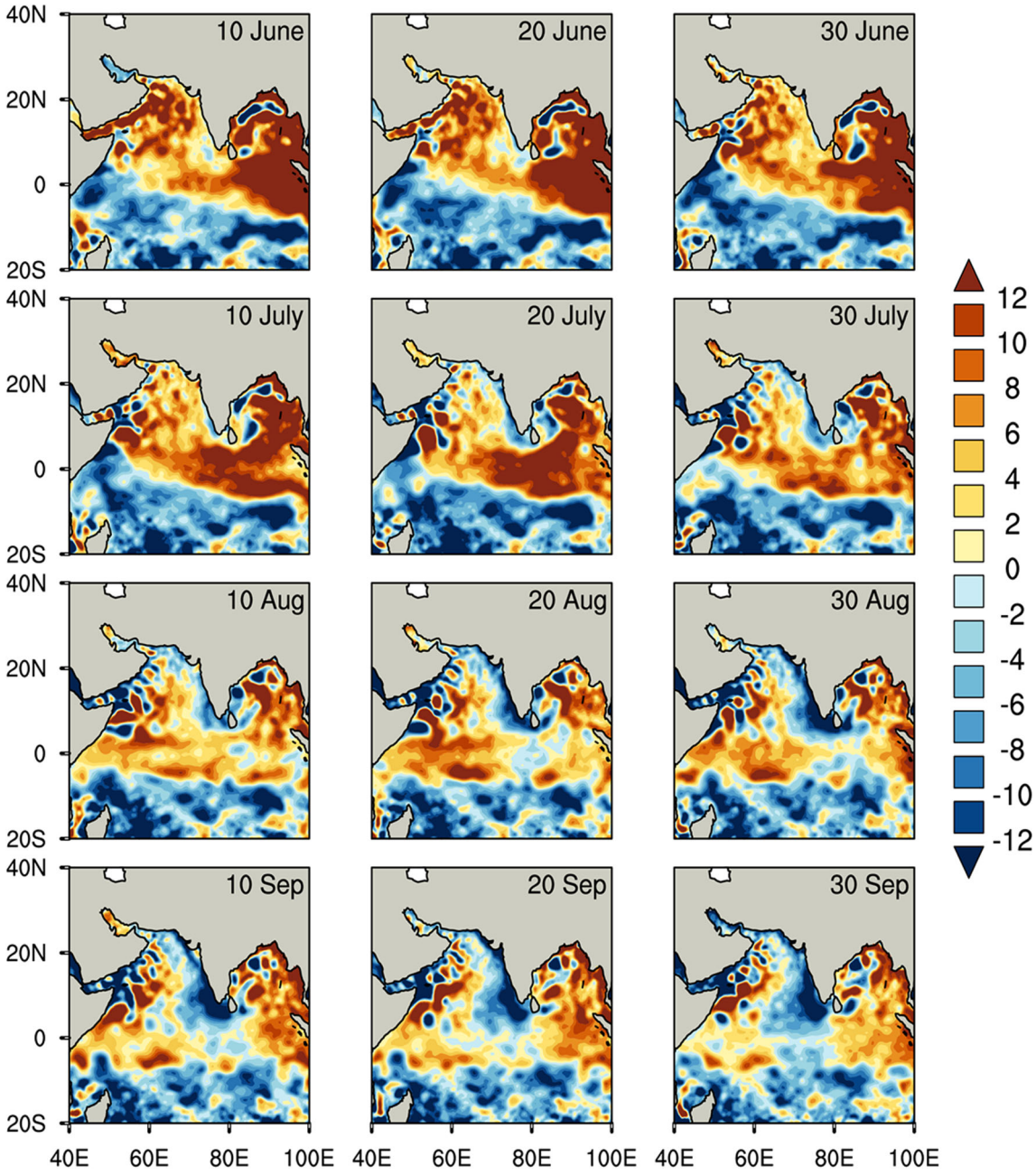

Fig. 7 SSHA (cm) using merged satellite data every 10 days from 10 June to 30 September during the year 2016

3.1.1 Spatial variation of JJAS rainfall and OLR

The spatial variations of JJAS rainfall anomalies over the Indian rainfall domain for the years 2016 and 2017 are shown in Fig. 3a–c. The highlighted domain indicates the monsoon core region. JJAS monsoon season of the year 2016 (2017) shows positive (negative) anomalies over the region. The difference (2016–2017) between contrasting monsoon (Fig. 3c) shows substantial positive anomalies surpassing 2 mm/day over this region as well as over the major part of the Indian landmass except in the northeast. The excess and deficient rainfall over the core monsoon region is unambiguous. Similarly, Fig. 4a–c shows spatial variations in OLR for the contrasting monsoon years. The OLR shows features similar to rainfall. Low OLR values are manifested over the land, and east Indian ocean in 2016 whereas in 2017, slight positive values over central India and increased values in the east IO are observed.

3.1.2 SSHA variability in the IO

Monthly and ten-day differences in SSHA (Figs. 6 and 7) are explored in addition to seasonal variability (Fig. 5) to extract short-term changes. Figure 5a, b depicts that JJAS SSHA

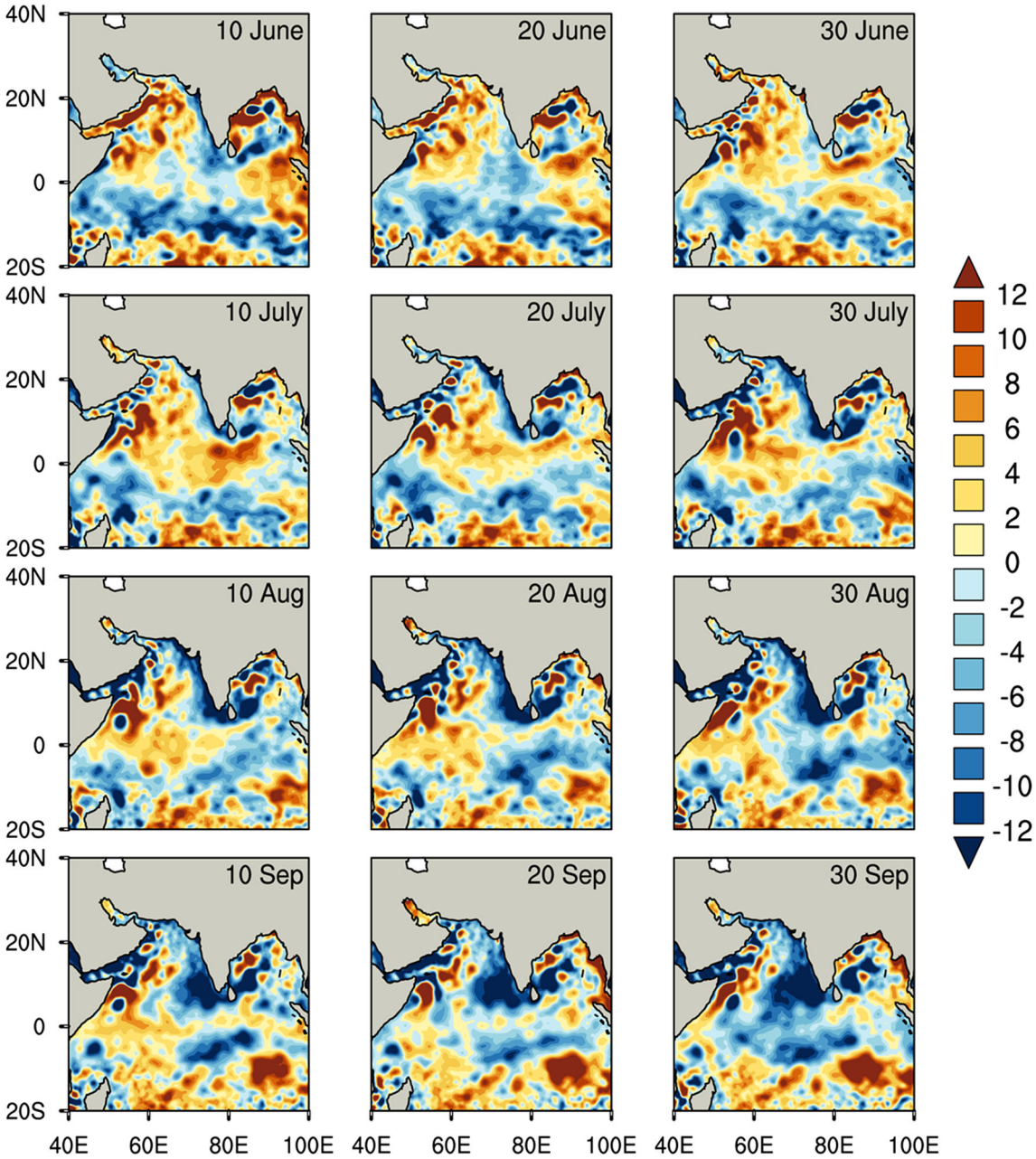

Fig. 8 Same as Fig. 7 for the year 2017

values were very high over the BoB in 2016 compared to 2017. In 2016, various regions of the IO north of 5S 5° S was occupied with positive SSHA (Fig. 5a). However, in 2017, more regions to the west of 90° E exhibit negative SSHA (Fig. 5b). The positive SSHA indicate a deep warm layer of the upper ocean, which corresponds to more heat content over that region. Therefore, tropical convection systems intensify rapidly in the areas of high SSHA (Fig. 6). Such systems forming in the BoB move westward resulting in rainfall over central India (Kripalani et al. 2007; Ajayamohan et al. 2010; Hunt et al. 2016; Hunt and Fletcher 2019). During June and July 2016, the SSHA is positive and exceeding 12 cm at various places over BoB, but when compared to June and July 2017, the magnitudes of SSHA were lower over the western BoB. During August and September 2017, negative SSHA occupied the western part of the BoB unlike August and September 2016. Over the eastern part of the BoB, very small patches of positive SSHA are seen, but the magnitude was lower during July to September 2017 compared to July to September 2016. Over the northern AS, the anomalies were positive from June to September in 2017, but the magnitude is higher than that from June to September 2017. Positive SSHA values imply higher heat content over the BoB in 2016 than in 2017. Ten-day interludes are examined to elucidate the modulation of the SSHA

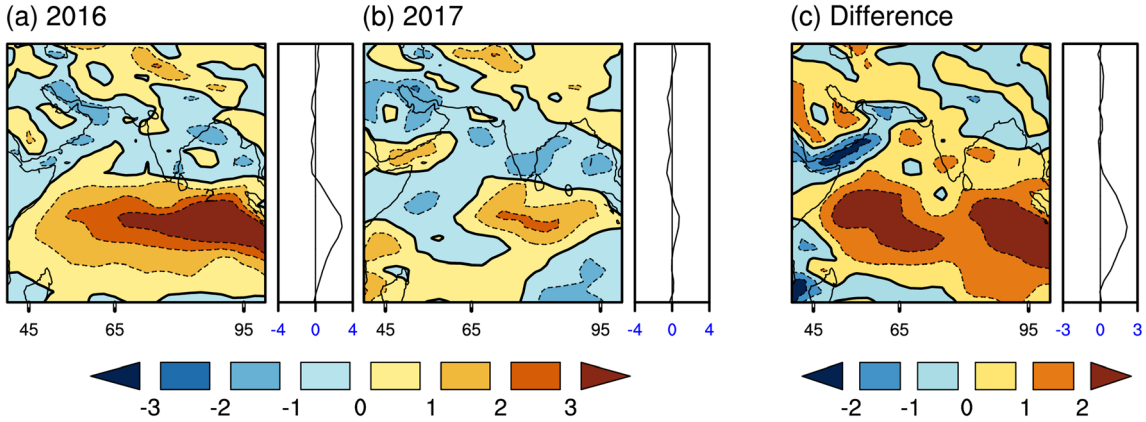

Fig. 9 JJAS surface zonal wind anomalies (ZWA) (m/s) for the years **a** 2016, **b** 2017, and **c** difference. The attached plot gives the information of the zonal average (40° E to 90° E) values of zonal wind

pattern evolution further (Figs. 7 and 8). Positive anomalies were getting subdued as the monsoon advanced in 2016, whereas the negative anomalies were enhanced in 2017. A large part of the BoB was covered with positive (negative) SSHA during whole monsoon season in 2016 (2017). Therefore, strong (feeble) convection over the BoB due to enhanced (suppressed) OHC resulted in predominantly positive (negative) SSHA values in 2016 (2017).

3.1.3 Surface zonal wind anomaly in the IO

The surface zonal wind anomaly (ZWA) values were positive with higher magnitudes over the equatorial region in 2016 as compared to 2017. The zonal average of the surface winds also depicts the same. The speed of ZWA is around 3.5 m/s (0.5 m/s) in 2016 (2017) over the equatorial region. Figure 9 shows that most of the IO were covered with positive surface ZWA in 2016 with the highest magnitudes over the equatorial region, which was not the case in 2017. Figure 10 shows that monthly surface ZWA values remain positive with higher magnitudes over the equatorial Indian ocean region in all months of 2016 whereas the signatures are not so secure in 2017 where the surface ZWA values were mostly negative. The planetary winds, equatorial KW and RW are driven by the remote forcing of the surface equatorial zonal winds (Potemra et al. 1991; McCreary et al. 1993). The equatorial KW on reaching the east coast of the IO reflect as equatorial RW and bifurcate into two coastal KW branches propagating poleward in the opposite directions. The northward limb travels along the eastern coastal rim of BoB. These coastal KWs, in turn, radiate westward propagating RW (Oliver and Thompson 2010; Rao et al. 2010a). The propagation of KW and RW in response to SSHA by the remote forcing of surface ZWA is mentioned in the next section.

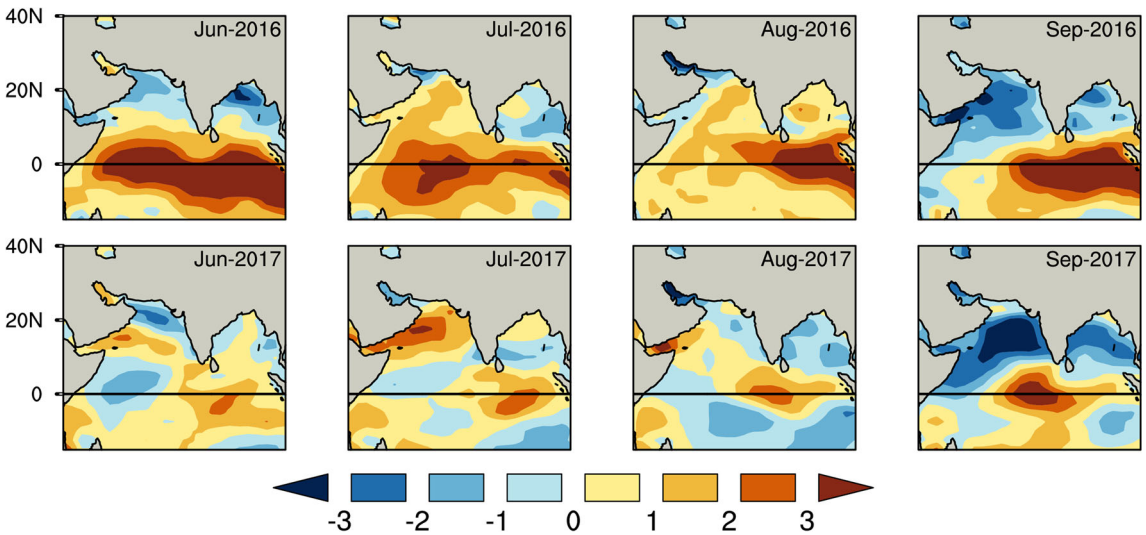

Fig. 10 The upper panel shows the surface zonal wind anomaly (ZWA) (m/s) from June to September during 2016 and the lower panel depicts the surface zonal wind anomaly (ZWA) (m/s) from June to September during 2017

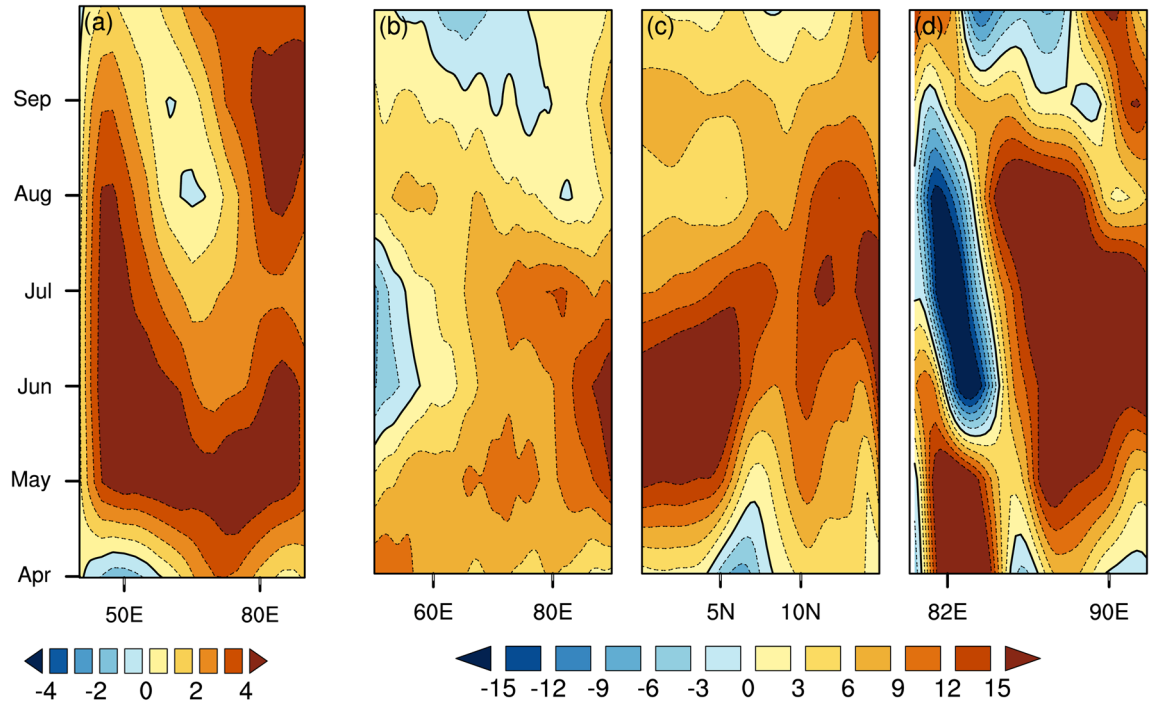

Fig. 11 **a** Equatorial ZWA from 40° E to 92° E, **b** equatorial SSHA from 50° E to 92° E, **c** SSHA along 90° E from the equator to 15° N, and **d** SSHA along 15° N from 92° E to 80° E during the period April to October 2016

3.1.4 Planetary-scale propagation of waves

The equatorial surface ZWA (2° N–2° S) were heavily westerly during the monsoon of 2016 (Fig. 9a) (Rao et al. 2010a) instigating a strong equatorial KW which propagated into the BoB that struck the east coast and continued as coastal KW towards either pole. Hence, strongly positive SSHAs were discerned along the equator and the eastern coast of BoB during JJAS 2016. Figures 11 and 12 show time-longitude (zonally averaged between 2° N and 2° S) sections of equatorial surface

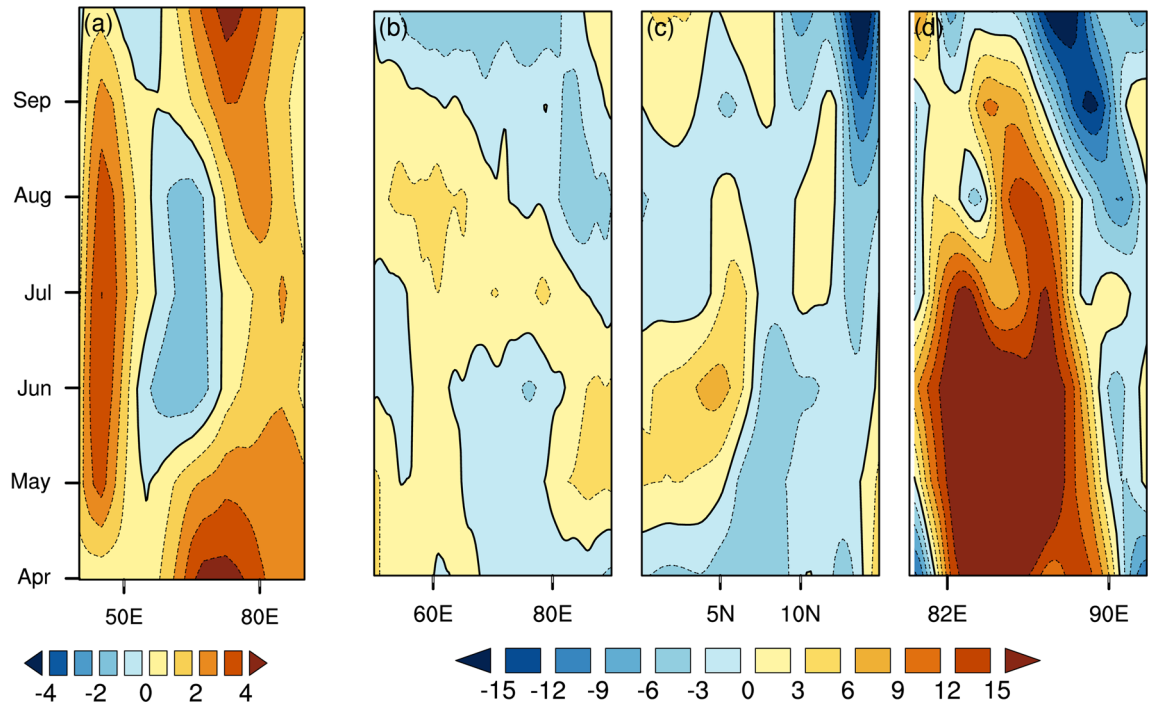

Fig. 12 Same as Fig. 11 for the year 2017

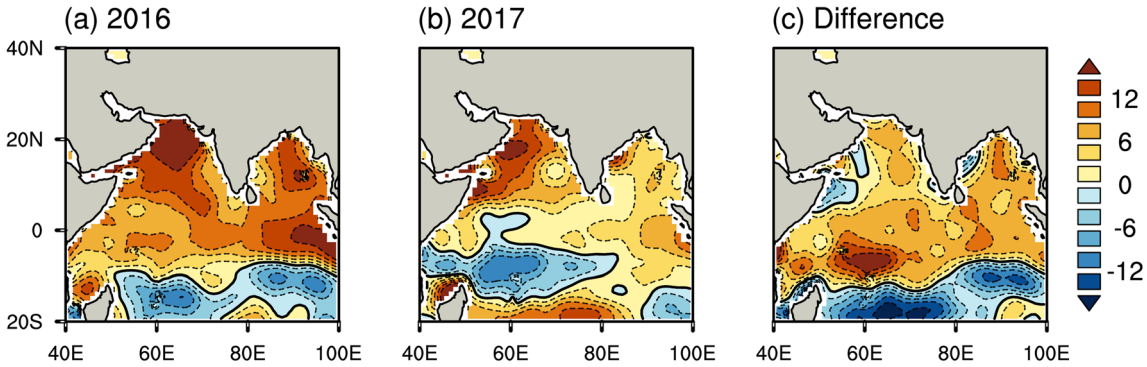

Fig. 13 JJAS ocean heat content anomaly (OHCA) ($\times 10^{18}$ J) during **a** 2016, **b** 2017, and **c** difference

ZWA and SSHA along the equatorial waveguide from 40° E to 92° E (equatorial KW), its northward progression (coastal KW) along 92°E from 0° N to 16° N, and westward progression (as RW) along 15° N from 92° E to 80° E during April to October 2016 and 2017. The downwelling and upwelling KW/RWs are rendered as positive and negative SSHA, respectively. During April 2016, the zonal winds initiate the downwelling KW from the western equatorial waveguide that reaches the east in June. Upon striking the east coast, these waves move back as downwelling RW (Fig. 11b) and also propagate in either hemisphere along the coastal rim (Fig. 11c). The downwelling RW goes along the equatorial waveguide and arrives on the western coast by mid-August. Throughout the monsoon season in 2016, the equatorial waveguide was manifested as downwelling KW and RW. The coastal downwelling KW along the east coastal rim of BoB radiated downwelling RWs (Fig. 11d). These downwelling RWs propagated westward into the BoB and inflated the SSHA values (Oliver and Thompson 2010; Rao et al. 2010a). The downwelling KW and RW result in greater heat content in the equatorial waveguide, the coastal rim of BoB, and in the interior BoB during the monsoon season.

However, during 2017, the equatorial surface ZWA were feeble over the west (Fig. 12a), resulting in a weak eastward equatorial KW propagation (Fig. 12b). Upwelling KW signatures were noticed from April to mid-July along 75° E prompting half-hearted RWs that reflect along the westward equatorial waveguide. The anomalies were easterlies from May to September along 60° E and were driving the upwelling KW. In the eastern coast, the upwelling KW propagates along the coastal rim and results in the generation of coastal upwelling KW (Fig. 12c), which further radiate upwelling RWs into the heart of BoB (Fig. 12d). In a nutshell, the upwelling KW and RW resulted in low heat content and negative SSHA values in the equatorial waveguide and BoB during the monsoon seasons.

3.1.5 Ocean heat content anomalies

The upper OHC plays an important role in the formation and intensification of the tropical convection systems. Rajeevan and McPhaden (2004)) have studied the interannual variability of the Pacific Ocean and its relation to ISMR. Parampil et al. (2010)) have studied the variation of the upper OHC on intraseasonal time scales in the BoB. The tropical systems maintain their intensity and grow in places where the SSHA and ocean heat content anomaly (OHCA) are high. The OHCA magnitudes over the northern IO were higher in 2016 than in 2017 (Fig. 13), though they were positive in both the years. Most of the northern IO exhibited SSHA values greater than 2 cm, especially in the BoB, where it surpassed

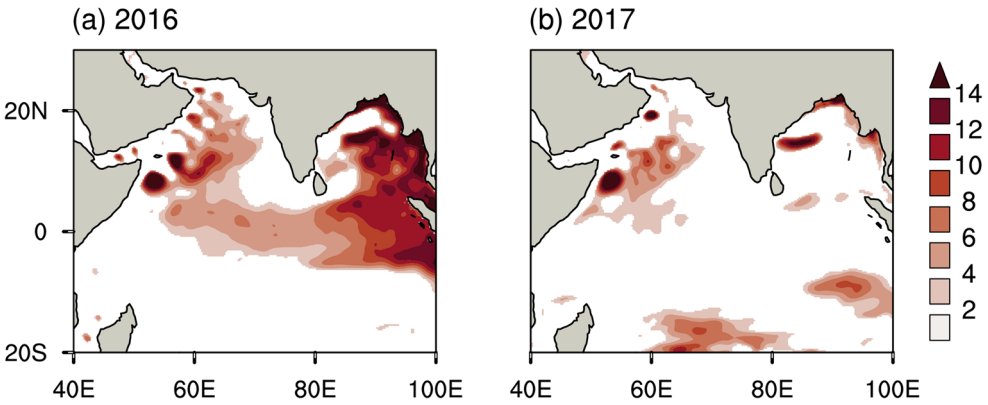

Fig. 14 Shaded region shows the JJAS SSHA greater than 2 cm for the years **a** 2016 and **b** 2017

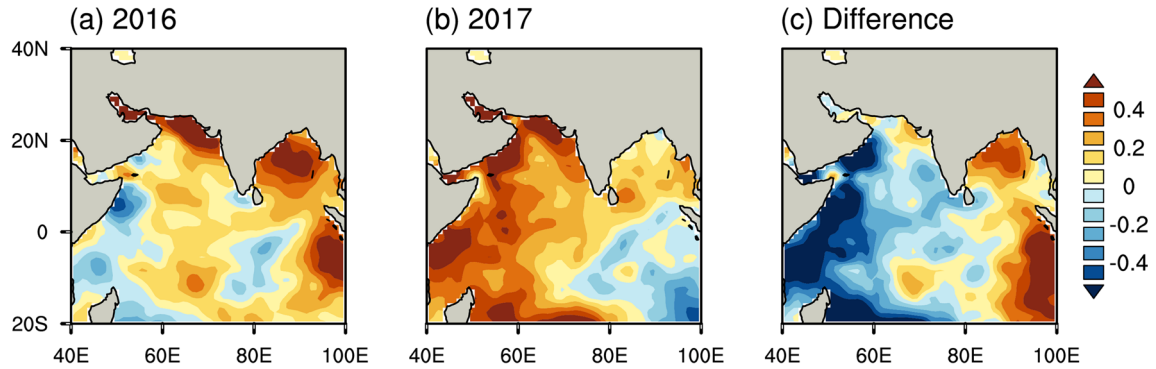

Fig. 15 JJAS sea surface temperature (SST) anomalies during **a** 2016, **b** 2017, and **c** difference

thresholds as high as 14 cm in 2016 (Fig. 14). However, 2017 witnessed only a few patches with SSHA greater than 2 cm in the northern IO. Therefore, in the places where OHCA values are robust and positive, SSHA values also get high and induce convective activities, ultimately causing more rainfall in the ocean and Indian landmass, especially over central India.

3.1.6 Sea surface temperature anomalies

During the whole monsoon period, the sea surface temperature (SST) over the BoB remains above 28 °C the threshold for convective systems. During JJAS 2016, the BoB witnessed positive SST anomalies, whereas the western IO have negative SST anomalies (Fig. 15a). However, the positive (negative) SST anomalies observed over the BoB (west IO) were feeble in magnitudes in JJAS 2017 (Fig. 15b). The difference between the two plots (Fig. 15c) indicates that in the previous year, warm anomalies were present along the east coast and BoB while cold anomalies filled the west coast and AS. The warm anomalies over the BoB were favorable for the evolution of low-pressure systems (LPS) due to enhanced convection. During the JJAS season, synoptic LPS form over the BoB and propagate west-northwestward, causing widespread rain over the subcontinent (Kripalani et al. 2007; Ajayamohan et al. 2010; Hunt et al. 2016; Hunt and Fletcher 2019).

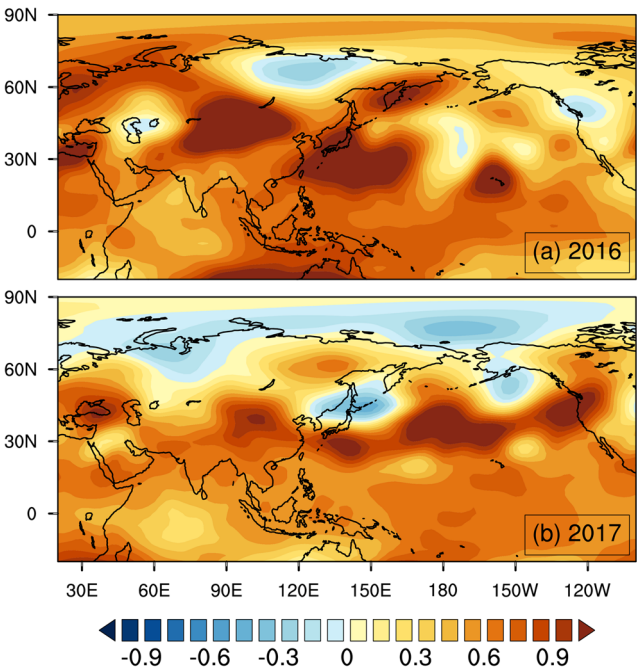

Fig. 16 JJAS tropospheric temperature (TT) anomalies (°C) during **a** 2016 and **b** 2017

3.2 Impact of atmospheric parameters during the two contrasting monsoon seasons

In this section, we examine the differences in atmospheric processes, their influences on the monsoonal rainfall during the two contrasting seasons, and plausible mechanisms behind.

3.2.1 Tropospheric temperature (600–200 hPa)

Xavier et al. (2007)) described the TT as the air temperature averaged between 600 and 200 hPa. The TT over the Indian landmass and Eurasia is one of the factors modulating the Indian monsoon rainfall, which was suggested by Liu and Yanai (2001)). Kothawale and Singh (2017)) studied TT trends over the Indian region using the radiosonde data and ascertained that the annual temperature trend from the surface to 500 hPa is increasing but from 200 to 150 hPa is decreasing over southern India, whereas in northern India, an increasing trend is seen at all pressure levels. TT is a valuable parameter for investigating the thermodynamic forcing related to monsoon (Xavier et al. 2007). We investigate the changes in the mean TT from 600 to 200 hPa during the contrasting monsoon years. Higher (lower) TT anomalies indicate a higher (lower) heat flux, which ultimately draws (retires) the moisture towards its core promoting stronger (weaker) rainfall. The TT anomalies during the two contrasting monsoon years are shown in Fig. 16. During 2016 monsoon season, TT shows higher values (Fig. 16a) which contributed to the high monsoon clouds and also responsible for luring more atmospheric moisture that caused convection over the Indian region through the mid-tropospheric heat flux. However, the signatures of TT values

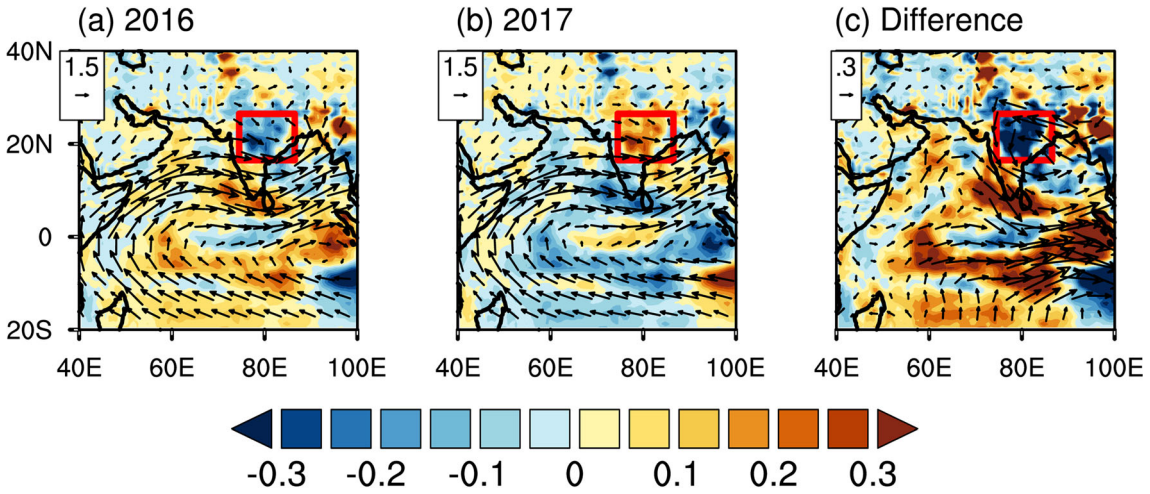

Fig. 17 Shaded region shows JJAS vertically integrated mass divergence/convergence anomaly from the surface to 300 hPa ($\times 10^{-4}$ kg/m^2/s; negative implies convergence and positive implies divergence) overlaid with JJAS moisture transport vectors (kg/m/s) for the years **a** 2016, **b** 2017, and **c** difference

are dim during 2017 (Fig. 16b), which results in a lesser influx of moisture and hence subdued rainfall.

3.2.2 Vertically integrated mass convergence/divergence and moisture transport vectors

To diagnose moisture transport as well as to understand the dynamical response of rainfall anomalies in the monsoon core region, vertically integrated moisture transport vectors during the two contrasting monsoon seasons are shown in Fig. 17. It is noted that during 2016 (Fig. 17a), most of the central Indian region, net convergence is dominant; however, during 2017 (Fig. 17b), the region shows net divergence. The moisture transport vectors show that easterlies from BoB help in feeding moisture to central India in 2016, whereas, in 2017, most of the transport is directed towards southern peninsular India (Fig. 17c). The high SSHA, SST, and OHCA over the BoB during 2016 result in enhanced evaporation and hence strengthened transport of moisture from the BoB to central Indian domain.

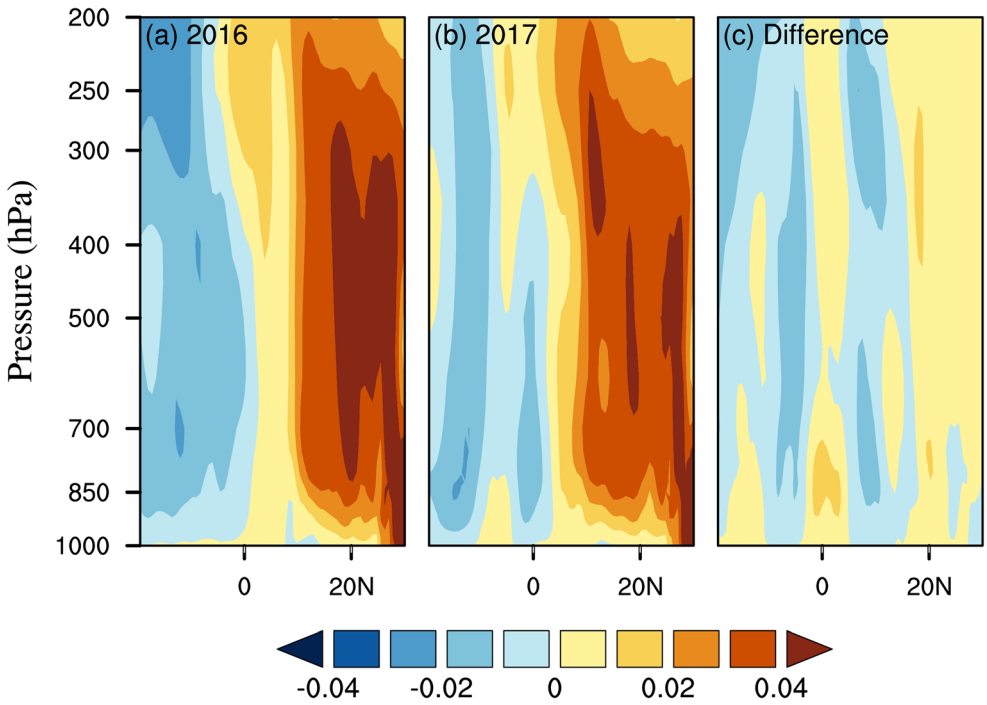

Fig. 18 JJAS pressure-latitude evolution of anomalous omega (pressure vertical velocity in hPa/s; multiplied by − 1.0) averaged over the longitude 60° E to 90° E (70°–85°E; 10°–25°N) during the years **a** 2016, **b** 2017, and **c** difference. Positive (negative) values represent ascending (descending) motion

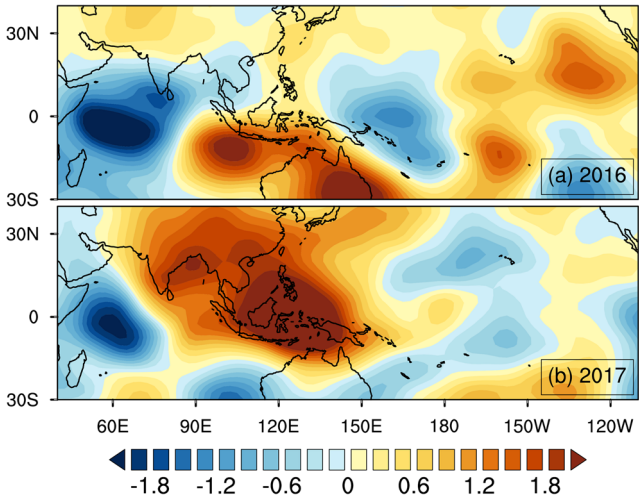

Fig. 19 JJAS velocity potential ($\times 10^{-6}$ m^2 s^{-1}) at 200 hPa during **a** 2016 and **b** 2017. Positive (negative) values represent upper-level convergence (divergence)

3.2.3 Vertical velocity from surface to 200 hPa

Vertical velocity is defined as the Lagrangian change of pressure with time, and the negative values represent cold advection (descending motion) whereas positive values represent warm advection (ascending motion). The pressure-latitude diagrams of vertical velocity averaged over 60° E to 90° E during the years 2016, 2017, and their difference are shown in Fig. 18a–c. The examination of vertical velocity during the contrasting years reveals a large-scale active ascending motion over central India (15°–25° N, selected box domain) and a weaker uplift/ascent over the equatorial regions in 2016 (Fig. 18a) as compared to 2017 (Fig. 18b). The difference diagram also implies the same (Fig. 18c). Larger values of vertical velocity over the highlighted domain resulted in extended lower level convection, which caused intensified rainfall over the domain during 2016.

3.2.4 Velocity potential at 200 hPa

The seasonal mean of velocity potential at 200 hPa, a parameter that reflects the tropical-meridional circulation, has been analyzed during the two contrasting monsoon years to quantify the changes in atmospheric circulation (Fig. 19). Negative values represent divergence (suitable for rainfall), whereas positive values indicate convergence (unbefitting for rainfall) at 200 hPa. In Fig. 19a, the eastern (western) Pacific is associated with upper-level convergence (divergence) that could intensify the Walker circulation and has a rising motion over the Indian subcontinent which is eventually auspicious for rainfall over the land. However, during 2017 (Fig. 19b), the eastern (western) Pacific is associated with upper-level divergence (convergence) that moderated the Walker circulation and had an anomalous subsiding branch over the Indian domain which finally abated the rainfall over the land.

4 Conclusion

The study mainly focuses on the importance of air-sea interaction processes in understanding the ISMR during two contrasting monsoon years, i.e., 2016 and 2017. Positive anomalies of SSHA are found to occupy most of the equatorial IO and BoB in 2016 (a typical monsoon year) and negative anomalies in 2017 (a deficient monsoon year). It has been established that the difference in variability is mainly due to the remote forcing by surface ZWA along the equator and is found to be a principal driver, which helps in the propagation

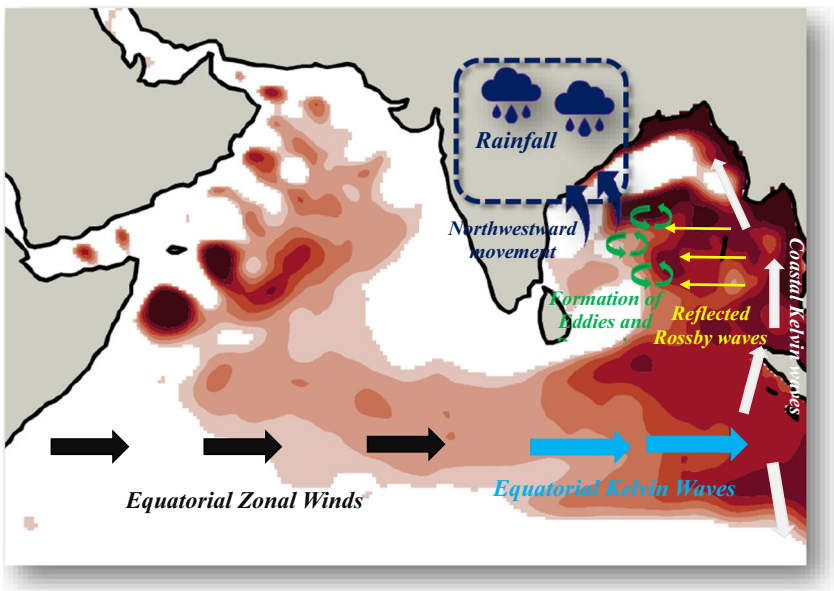

Fig. 20 A schematic diagram represents different oceanic components during the year 2016. The shading shows the JJAS 2016 SSHA greater than 2 cm and different arrows determine the multiple processes that result in the high precipitation over central India during 2016

of planetary-scale waves. During the 2016 monsoon, anomalous equatorial westerlies have driven downwelling KW along the equatorial waveguide which on reaching the east coast bifurcate into coastal KW. These coastal KW travel along the coastal rim of BoB and also radiate RW that propagate into the interior of BoB and result in high ocean heat content. On the other hand, the equatorial forcing was opposite with anomalous easterlies resulting in upwelling KW and RW along the equatorial waveguide and interior of BoB in 2017. The consequence was positive SSHA values with larger magnitudes in the equatorial waveguide and interior of BoB in 2016 compared to 2017. The differences in the SSHA during the two monsoon seasons possibly lead to enhanced convection and formation of lows and depression in the BoB in 2016 and subdued convective activities next year. SST and OHCA also found to be higher in the BoB that resulted in accelerated evaporation and therefore strengthened moisture transport into central India. Figure 20 represents the whole physical mechanism of different oceanic components during the year 2016.

During the monsoon season of 2016, a high TT was responsible for drawing in more moisture and causing convection over the Indian region through the mid-tropospheric heat flux, whereas lower values of TT in 2017 weakened the moisture influx. Also, the positive TT values over the Eurasian region provided a conducive environment for large-scale convection over the Indian subcontinent. A net convergence dominated the central Indian domain in 2016 while the region had a net divergence in the year followed. Moisture transport vectors show that easterlies from BoB helped to feed the moisture into the central Indian landmass causing intense rainfall over the region. Large positive values of vertical velocity at all pressure levels resulted in a large-scale ascending motion between 15° N and 25° N. Velocity potential at 200 hPa also depicts the upper-level convergence (divergence) in the eastern Pacific that strengthened (weaken) the Walker circulation and upper-level divergence (convergence) and anomalous rising (subsiding) motion over India in the year 2016 (2017).

This study brings out the importance of air-sea processes and interactions in understanding the rainfall on the backdrop of two contrasting monsoon seasons. However, regional air-sea interaction model simulations would be required to confirm the hypothesis.

Funding information The first author is thankful to Dept. of Science and Technology (DST), Govt. of India for supporting the junior research fellowship via grant number DST/CCP/NCM/69/2017. AM and MSS acknowledge INSPIRE PhD fellowship from DST grant no. IF170016 and IF160281, respectively. PK recognizes the funding from the Science and Engineering Research Board (SERB), Govt. of India, grant number SB/S2/RJN-080/2014, and DST grant number DST/CCP/NCM/69/2017.

Data availability SSHA dataset can be found at https://www.aviso.altimetry.fr/en/data/products/sea-surface-height-products.html, GPCP precipitation dataset is available at https://psl.noaa.gov/data/gridded/data.gpcp.html, NCEP/NCAR data is available at https://psl.noaa.gov/data/gridded/data.ncep.reanalysis.pressure.html, Era-Interim dataset can be found at https://www.ecmwf.int/en/forecasts/datasets/reanalysis-datasets/era-interim, and NODC data for ocean heat content is available at https://www.nodc.noaa.gov/OC5/3M_HEAT_CONTENT/

References

Ajayamohan RS, Merryfield WJ, Kharin VV (2010) Increasing trend of synoptic activity and its relationship with extreme rain events over central India. J Clim 23:1004–1013. https://doi.org/10.1175/2009JCLI2918.1

Alory G, Meyers G (2009) Warming of the upper equatorial Indian Ocean and changes in the heat budget (1960-99). J Clim 22:93–113. https://doi.org/10.1175/2008JCLI2330.1

Annamalai H, Murtugudde R, Potemra J, et al (2003) Coupled dynamics over the Indian Ocean: spring initiation of the zonal mode. Deep Res Part II Top Stud Oceanogr. doi: https://doi.org/10.1016/S0967-0645(03)00058-4

Ashok K, Guan Z, Yamagata T (2001) Impact of the Indian Ocean dipole on the relationship between the Indian monsoon rainfall and ENSO. Geophys Res Lett 28:4499–4502. https://doi.org/10.1029/2001GL013294

Bhatla R, Raju PVS, Mohanty UC, Madan OP, Mall RK (2011) Study of energy fluxes over the Indian ocean prior and during the summer monsoon. Mar Geod 34:119–137. https://doi.org/10.1080/01490419.2011.571557

Brandt P, Stramma L, Schott F, Fischer J, Dengler M, Quadfasel D (2002) Annual Rossby waves in the Arabian Sea from TOPEX/POSEIDON altimeter and in situ data. Deep Res Part II Top Stud Oceanogr. 49:1197–1210. https://doi.org/10.1016/S0967-0645(01)00166-7

Chelton DB, Schlax MG (1996) Global observations of oceanic Rossby waves. Science (80-). doi: https://doi.org/10.1126/science.272.5259.234

Chowdary JS, Gnanaseelan C, Xie SP (2009) Westward propagation of barrier layer formation in the 2006-07 Rossby wave event over the tropical southwest Indian Ocean. Geophys Res Lett 36. https://doi.org/10.1029/2008GL036642

Emanuel KA (1999) Thermodynamic control of hurricane intensity. Nature. 401:665–669. https://doi.org/10.1038/44326

Feng M, Meyers G (2003) Interannual variability in the tropical Indian Ocean: a two-year time-scale of Indian Ocean Dipole. Deep Res Part II Top Stud Oceanogr 50:2263–2284. https://doi.org/10.1016/S0967-0645(03)00056-0

Feng M, Meyers G, Wijffels S (2001) Interannual upper ocean variability in the tropical Indian Ocean. Geophys Res Lett 28:4151–4154. https://doi.org/10.1029/2001GL013475

Gadgil S, Joseph PV, Joshi NV (1984) Ocean-atmosphere coupling over monsoon regions. Nature. 312:141–143. https://doi.org/10.1038/312141a0

Gadgil S, Vinayachandran PN, Francis PA, Gadgil S (2004) Extremes of the Indian summer monsoon rainfall, ENSO and equatorial Indian Ocean oscillation. Geophys Res Lett doi: https://doi.org/10.1029/2004GL019733, 31

Gera A, Mitra AK, Mahapatra DK, Momin IM, Rajagopal EN, Basu S (2016) Sea surface height anomaly and upper ocean temperature over the Indian Ocean during contrasting monsoons. Dyn Atmos Ocean. 75:1–21. https://doi.org/10.1016/j.dynatmoce.2016.04.002

Goswami BN (1998) The physics of ENSO-monsoon connection. Indian J Mar Sci

Goswami BN, Ajayamohan RS, Xavier PK, Sengupta D (2003) Clustering of synoptic activity by Indian summer monsoon intraseasonal oscillations. Geophys Res Lett 30. https://doi.org/10.1029/2002GL016734

Han W, Meehl GA, Rajagopalan B, Fasullo JT, Hu A, Lin J, Large WG, Wang JW, Quan XW, Trenary LL, Wallcraft A, Shinoda T, Yeager S (2010) Patterns of Indian Ocean sea-level change in a warming climate. Nat Geosci 3:546–550. https://doi.org/10.1038/ngeo901

Hunt KMR, Turner AG, Inness PM, Parker DE, Levine RC (2016) On the structure and dynamics of Indian monsoon depressions. Mon Weather Rev 144:3391–3416. https://doi.org/10.1175/MWR-D-15-0138.1

Hunt KMR, Fletcher JK (2019) The relationship between Indian monsoon rainfall and low-pressure systems. Clim Dyn 53:1859–1871. https://doi.org/10.1007/s00382-019-04744-x

India Meteorological Department (2017) 2017 southwest monsoon end of season report. Earth Syst Sci Organ Minist Earth Sci India Meteorol Dep

India Meteorological Department (2016) 2016 southwest monsoon end of season report. Earth Syst Sci Organ Minist Earth Sci India Meteorol Dep

Joseph S, Sahai AK, Dey A, Mandal R, Aparnna RP (2018) On the dynamics of extended breaks during 2017 monsoon. Research Report No. RR-143. ESSO/IITM/SERP/SR/05(2018)/194

Kantha L, Rojsiraphisal T, Lopez J (2008) The North Indian Ocean circulation and its variability as seen in a numerical hindcast of the years 1993-2004. Prog Oceanogr 76:111–147. https://doi.org/10.1016/j.pocean.2007.05.006

Keshavamurty RN (1982) Response of the atmosphere to sea surface temperature anomalies over the equatorial Pacific and the teleconnections of the Southern Oscillation. J Atmos Sci 39:1241–1259. https://doi.org/10.1175/1520-0469(1982)039<1241:rotats>2.0.co;2

Kothawale DR, Singh HN (2017) Recent trends in tropospheric temperature over India during the period 1971–2015. Earth Sp Sci 4:240–246. https://doi.org/10.1002/2016EA000246

Kripalani RH, Oh JH, Kulkarni A, Sabade SS, Chaudhari HS (2007) South Asian summer monsoon precipitation variability: coupled climate model simulations and projections under IPCC AR4. Theor Appl Climatol 90:133–159. https://doi.org/10.1007/s00704-006-0282-0

Krishnamurthy V, Goswami BN (2000) Indian monsoon-ENSO relationship on interdecadal timescale. J Clim 13:579–595. https://doi.org/10.1175/1520-0442(2000)013<0579:IMEROI>2.0.CO;2

Krishnamurti TN, Oosterhof DK, Mehta AV (1988) Air–sea interaction on the time scale of 30 to 50 days. J Atmos Sci 45:1304–1322. https://doi.org/10.1175/1520-0469(1988)045<1304:aiotts>2.0.co;2

Kumar MRR, Sathyendranath S, Viswambharan NK, Rao LVG (1986) Sea surface temperature variability over North Indian Ocean—a study of two contrasting monsoon seasons. Proc Indian Acad Sci - Earth Planet Sci. 95:435–446. https://doi.org/10.1007/BF02842510

Liu X, Yanai M (2001) Relationship between the Indian monsoon rainfall and the tropospheric temperature over the Eurasian continent. Q J R Meteorol Soc 127:909–937. https://doi.org/10.1256/smsqj.57310

Masumoto Y, Meyers G (1998) Forced Rossby waves in the southern tropical Indian Ocean. J Geophys Res Ocean 103:27589–27602. https://doi.org/10.1029/98JC02546

McCreary JP, Kundu PK, Molinari RL (1993) A numerical investigation of dynamics, thermodynamics and mixed-layer processes in the Indian Ocean. Prog Oceanogr 31:181–244

Meyers G (1996) Variation of Indonesian throughflow and the El Niño-Southern Oscillation. J Geophys Res C Ocean. 101:12255–12263. https://doi.org/10.1029/95JC03729

Murtugudde R, McCreary JP, Busalacchi AJ (2000) Oceanic processes associated with anomalous events in the Indian Ocean with relevance to 1997-1998. J Geophys Res Ocean. 105:3295–3306. https://doi.org/10.1029/1999jc900294

Oliver ECJ, Thompson KR (2010) Madden-Julian oscillation and sea level: local and remote forcing. J Geophys Res Ocean. 115. https://doi.org/10.1029/2009JC005337

Pant GB, Parthasarathy SB (1981) Some aspects of an association between the southern oscillation and Indian summer monsoon. Arch Meteorol Geophys Bioclimatol Ser B 29:245–252. https://doi.org/10.1007/BF02263246

Parampil SR, Gera A, Ravichandran M, Sengupta D (2010) Intraseasonal response of mixed layer temperature and salinity in the Bay of Bengal to heat and freshwater flux. J Geophys Res Ocean. 115. https://doi.org/10.1029/2009JC005790

Peter BN, Mizuno K (2000) Annual cycle of steric height in the Indian Ocean estimated from the thermal field. Deep Res Part I Oceanogr Res Pap 47:1351–1368. https://doi.org/10.1016/S0967-0637(99)00088-6

Polito PS (1997) Long baroclinic Rossby waves detected by TOPEX/POSEIDON. J Geophys Res C Ocean 102:3215–3235. https://doi.org/10.1029/96JC03349

Potemra JT, Luther ME, O'Brien JJ (1991) The seasonal circulation of the upper ocean in the Bay of Bengal. J Geophys Res 96:12667. https://doi.org/10.1029/91jc01045

Rajeevan M, McPhaden MJ (2004) Tropical Pacific upper ocean heat content variations and Indian summer monsoon rainfall. Geophys Res Lett 31. https://doi.org/10.1029/2004GL020631

Raju PVS, Mohanty UC, Rao PLS, Bhatla R (2002) The contrasting features of Asian summer monsoon during surplus and deficient rainfall over India. Int J Climatol 22:1897–1914. https://doi.org/10.1002/joc.855

Ramesh Kumar MR, Shenoi SSC, Schulz J (2005) Impact of convection over the equatorial trough on summer monsoon activity over India. Int J Remote Sens 26:4747–4762. https://doi.org/10.1080/01431160500196414

Rao RR, Girish Kumar MS, Ravichandran M, Rao AR, Gopalakrishna VV, Thadathil P (2010b) Interannual variability of Kelvin wave propagation in the wave guides of the equatorial Indian Ocean, the coastal Bay of Bengal and the southeastern Arabian Sea during 1993-2006. Deep Res Part I Oceanogr Res Pap. 57:1–13. https://doi.org/10.1016/j.dsr.2009.10.008

Rao RR, Sivakumar R (2000) Seasonal variability of near-surface thermal structure and heat budget of the mixed layer of the tropical Indian Ocean from a new global ocean temperature climatology. J Geophys Res Ocean. 105:995–1015. https://doi.org/10.1029/1999jc900220

Rao SA, Behera SK, Masumoto Y, Yamagata T (2002) Interannual subsurface variability in the tropical Indian Ocean with a special emphasis on the Indian Ocean Dipole. Deep Res Part II Top Stud Oceanogr. 49:1549–1572. https://doi.org/10.1016/S0967-0645(01)00158-8

Rao SA, Chaudhari HS, Pokhrel S, Goswami BN (2010a) Unusual central Indian drought of summer monsoon 2008: role of southern tropical Indian Ocean warming. J Clim 23:5163–5174. https://doi.org/10.1175/2010JCLI3257.1

Sadhuram Y, Rao BP, Rao DP, Shastri PNM, Subrahmanyam MV (2004) Seasonal variability of cyclone heat potential in the Bay of Bengal. Nat Hazards 32:191–209. https://doi.org/10.1023/B:NHAZ.0000031313.43492.a8

Saji NH, Goswami BN, Vinayachandran PN, Yamagata T (1999) A dipole mode in the tropical Indian ocean. Nature. 401:360–363. https://doi.org/10.1038/43854

Schiller A, Wijffels SE, Sprintall J, Molcard R, Oke PR (2010) Pathways of intraseasonal variability in the Indonesian Throughflow region. Dyn Atmos Ocean 50:174–200. https://doi.org/10.1016/j.dynatmoce.2010.02.003

Sengupta D, Goswami BN, Senan R (2001) Coherent intraseasonal oscillations of ocean and atmosphere during the Asian summer monsoon. Geophys Res Lett 28:4127–4130. https://doi.org/10.1029/2001GL013587

Sengupta D, Ravichandran M (2001) Oscillations of Bay of Bengal sea surface temperature during the 1998 summer monsoon. Geophys Res Lett 28:2033–2036. https://doi.org/10.1029/2000GL012548

Shankar D, Shetye SR, Joseph PV (2007) Link between convection and meridional gradient of sea surface temperature in the Bay of Bengal. J Earth Syst Sci 116:385–406. https://doi.org/10.1007/s12040-007-0038-y

Shukla J, Paolino DA (2002) The southern oscillation and long-range forecasting of the summer monsoon rainfall over India. Mon Weather Rev 111:1830–1837. https://doi.org/10.1175/1520-0493(1983)111<1830:tsoalr>2.0.co;2

Sikka DR (1980) Some aspects of the large scale fluctuations of summer monsoon rainfall over India in relation to fluctuations in the planetary and regional scale circulation parameters. Proc Indian Acad Sci - Earth Planet Sci 89:179–195. https://doi.org/10.1007/BF02913749

Sreejith OP, Panickal S, Pai S, Rajeevan M (2015) An Indian Ocean precursor for Indian summer monsoon rainfall variability. Geophys Res Lett 42:9345–9354. https://doi.org/10.1002/2015GL065950

Subrahmanyam B, Robinson IS, Blundell JR, Challenor PG (2001) Indian ocean Rossby waves observed in TOPEX/POSEIDON altimeter data and in model simulations. Int J Remote Sens 22:141–167. https://doi.org/10.1080/014311601750038893

Trenary LL, Han W (2012) Intraseasonal-to-interannual variability of South Indian Ocean sea level and thermocline: remote versus local forcing. J Phys Oceanogr 42:602–627. https://doi.org/10.1175/jpo-d-11-084.1

Vecchi GA, Harrison DE (2002) Monsoon breaks and subseasonal sea surface temperature variability in the Bay of Bengal. J Clim 15:1485–1493. https://doi.org/10.1175/1520-0442(2002)015<1485:MBASSS>2.0.CO;2

Venugopal T, Ali MM, Bourassa MA, Zheng Y, Goni GJ, Foltz GR, Rajeevan M (2018) Statistical evidence for the role of southwestern Indian Ocean heat content in the Indian summer monsoon rainfall. Sci Rep 8:12092. https://doi.org/10.1038/s41598-018-30552-0

Walker GT, Bliss EW (1932) World Weather V—NAO. Mem R Meteorol Soc

Wang JW, Han W, Sriver RL (2012) Impact of tropical cyclones on the ocean heat budget in the Bay of Bengal during 1999: 1. Model configuration and evaluation. J Geophys Res Ocean. https://doi.org/10.1029/2012JC008372

Webster PJ, Magaña VO, Palmer TN, Shukla J, Tomas RA, Yanai M, Yasunari T (1998) Monsoons: processes, predictability, and the prospects for prediction. J Geophys Res Ocean. 103:14451–14510. https://doi.org/10.1029/97jc02719

Webster PJ, Moore AM, Loschnigg JP, Leben RR (1999) Coupled ocean-atmosphere dynamics in the Indian Ocean during 1997-98. Nature. 401:356–360. https://doi.org/10.1038/43848

Xavier PK, Marzin C, Goswami BN (2007) An objective definition of the Indian summer monsoon season and a new perspective on the ENSO-monsoon relationship. Q J R Meteorol Soc 133:749–764. https://doi.org/10.1002/qj.45

Yang J, Yu L, Koblinsky CJ, Adamec D (1998) Dynamics of the seasonal variations in the Indian Ocean from TOPEX/POSEIDON sea surface height and an ocean model. Geophys Res Lett 25:1915–1918. https://doi.org/10.1029/98gl01401

Yu L, McPhaden MJ (2011) Ocean preconditioning of Cyclone Nargis in the Bay of Bengal: interaction between Rossby waves, surface fresh waters, and sea surface temperatures. J Phys Oceanogr 41:1741–1755. https://doi.org/10.1175/2011jpo4437.1